Photoinduced Ferrimagnetic Systems in Prussian Blue Analogues $C^I_xCo_4[Fe(CN)_6]_y$ (C^I = Alkali Cation). 2. X-ray Absorption Spectroscopy of the Metastable State

Christophe Cartier dit Moulin,*,†,‡ Françoise Villain,†,‡ Anne Bleuzen,*,† Marie-Anne Arrio,§ Philippe Sainctavit,§ Claire Lomenech,† Virginie Escax,† François Baudelet,‡ Elizabeth Dartyge,‡ Jean-Jacques Gallet,‡,† and Michel Verdaguer†

Contribution from the Laboratoire de Chimie Inorganique et Matériaux Moléculaires, Unité CNRS 7071, Université Pierre et Marie Curie, 4 place Jussieu, Bât F, 75252 Paris Cedex 05, France, Laboratoire pour l'Utilisation du Rayonnement Electromagnétique, UMR CNRS 130-CEA-MEN, Bât. 209 D, BP 34, 91898 Orsay Cedex, France, Laboratoire de Minéralogie Cristallographie, UMR CNRS 7590, UPMC/UDD/IPGP, 4 place Jussieu, 75252 Paris Cedex 05, France, and Laboratoire de Chimie Physique, UMR CNRS 7614, Université Pierre et Marie Curie, 11 rue Pierre et Marie Curie, 75 231 Paris Cedex 05, France

Received January 31, 2000

Abstract: A CoFe Prussian blue analogue $Rb_{1.8}Co_4[Fe(CN)_6]_{3.3}\cdot 13H_2O$ was synthesized, which presents an important photomagnetic effect. The electronic structure and the local structure of the ground and of the excited states have been investigated. X-ray absorption spectroscopy measurements at the Co and Fe $L_{2,3}$ edges and cobalt K-edge (XANES and EXAFS) evidence the local electronic transfer and the spin change of the cobalt ions induced by irradiation. We observed a 0.19 Å increase of the Co−N bond length, associated with the transformation of Co^{III} low spin to Co^{II} high spin. The Co^{II}/Co^{III} ratio has been evaluated as a function of the irradiation time and revealed as an important parameter to understanding the bulk magnetic properties. The combined role of the diamagnetic $Fe^{II}-Co^{III}$ pairs and hexacyanoferrate(III) vacancies is locally evidenced. This work is a new step in the understanding of the photoinduced electron transfer.

Introduction

The photoinduced magnetization in a Prussian blue analogue evidenced by Hashimoto and co-workers in 1996[1−4] and further studied by the same group has been explained by the presence of diamagnetic $Fe^{II}-Co^{III}$ pairs in the compound and a photoinduced electron transfer from Fe^{II} to Co^{III} through the cyanide bridge.[1,5,6] In part 1, we correlated the number of diamagnetic pairs to the intensity of the photoinduced magnetization effect. To do that, we synthesized in particular the compound formulated $Rb_{1.8}Co_4[Fe(CN)_6]_{3.3}\cdot 13H_2O$ (compound **2** in part 1, here abbreviated $Rb_{0.5}CoFe$), which presents an important photoinduced magnetization.[7] We demonstrated that the presence of diamagnetic pairs is a necessary but not a sufficient condition to observe the phenomenon.[7] To go deeper in the understanding of the photoinduced magnetization, we have characterized the electronic and local structures of the ground and excited states in $Rb_{0.5}CoFe$ to get an understanding of the photoinduced magnetization. We present here X-ray absorption spectroscopy measurements at the Co and at the Fe $L_{2,3}$ edges to study the electronic structure and at the cobalt K-edge to study the local structure around the cobalt. Given the similarity of the crystallographic structures of $K_3[Fe^{III}(CN)_6]$ and $K_4[Fe^{II}(CN)_6]$,[8] the iron K-edge was not investigated. The characterization of the local and the electronic structure of the photoexcited state allows progress in the understanding of the photoinduced electron-transfer mechanism.

Experimental Section

Materials. The compound $Rb_{1.8}Co_4[Fe(CN)_6]_{3.3}\cdot 13H_2O$ ($Rb_{0.5}CoFe$) was synthesized as described in part 1.[7] It displays 82.5% of $Fe^{II}-CN-Co^{III}$ diamagnetic pairs and 17.5% of Co^{II} associated with hexacyanoferrate vacancies. The rubidium cations occupy about a quarter of the tetrahedral interstitial sites.[7]

The model compounds $K_3[Fe^{III}(CN)_6]$, $K_4[Fe^{II}(CN)_6]$, $K_3[Co^{III}(CN)_6]$, and $[Co^{II}(H_2O)_6](NO_3)_2$ were purchased from Merck and used as received.

XAS Data Collection. The soft X-ray experiments were performed on the soft X-ray storage ring Super-ACO at LURE (Orsay, France). The Fe and Co $L_{2,3}$ edges were recorded on the SU23 beamline where the monochromator is a plane grating.[9] The powder samples were layed

† Université Pierre et Marie Curie.
‡ Laboratoire pour l'Utilisation du Rayonnement Electromagnétique.
§ Laboratoire de Minéralogie Cristallographie.

(1) Sato, O.; Iyoda, T.; Fujishima, A.; Hashimoto, K. *Science* **1996**, *272*, 704−705.
(2) Sato, O.; Einaga, Y.; Iyoda, T.; Fujishima, A.; Hashimoto, K. *J. Electrochem. Soc.* **1997**, *144*, L11−L13.
(3) Sato, O.; Einaga, Y.; Iyoda, T.; Fujishima, A.; Hashimoto, K. *J. Phys. Chem. B* **1997**, *101*, 3903−3905.
(4) (a) Einaga, Y.; Ohkoshi, S.-I.; Sato, O.; Fujishima, A.; Hashimoto, K. *Chem. Lett.* **1998**, 585−586. (b) Sato, O.; Einaga, Y.; Fujishima, A.; Hashimoto, K. *Inorg. Chem.* **1999**, *38*, 4405−4412.
(5) Verdaguer, M. *Science* **1996**, *272*, 698−699.
(6) Bleuzen, A.; Lomenech, C.; Dolbecq, A.; Villain, F.; Goujon, A.; Roubeau, O.; Nogues, M.; Varret, F.; Baudelet, F.; Dartyge, E.; Giorgetti, C.; Gallet, J. J.; Cartier dit Moulin, C.; Verdaguer, M. *Mol. Cryst. Liq. Cryst.* **1999**, *335*, 965−974.
(7) Part 1: Bleuzen, A.; Lomenech, C.; Escax, V.; Villain, F.; Varret, F.; Cartier dit Moulin, C.; Verdaguer, M. *J. Am. Chem. Soc.* **2000**, *122*, 6648−6652.
(8) Weiser, H. B.; Milligan, W. O.; Bates, J. B. *J. Phys. Chem.* **1942**, *46*, 99−106.
(9) Hague, C. F.; Mariot, J. M.; Guo, G. Y.; Hricovini, H.; Krill, G. *Phys. Rev. B* **1995**, *51*, 1370−1373.

10.1021/ja000349m CCC: $19.00
Published on Web 06/30/2000

on a grid carved on a copper metal sheet. The spectra were recorded by measuring the photocurrent emitted by the sample under a vacuum of at least 10^{-9} mbar. The detection is a total yield detection mode, hence the measure is surface sensitive (a few tens Å) due to the escape depth of the electrons. The sample has been cooled to 20 ± 3 K.

X-ray Absorption Near Edge Spectroscopy (XANES) measurements were performed at the cobalt K-edge using the energy dispersive absorption beamline of the DCI ring at LURE (Orsay), using a Si 111 curved polychromator, focusing 70 cm at the sample position. The edge energy of the cobalt at 7709 eV was fixed at the first inflection point of the metallic foil. The recording temperature was $T = 300$ and about 30 K. The X-ray absorption spectra were recorded by measuring the photocurrent emitted by the photodiodes. In this experimental geometry, thin samples are needed (4 mg of product dispersed on a 1 cm^2 Millipore membrane): in this way, we increase the percentage of transformed compound, by increasing the penetration depth of the visible light. In this transmission mode detection, surface and bulk of the sample are probed. The disadvantage of this recording mode is the reduced energy range scanned (up to 8 $Å^{-1}$ in k), compared to a step by step Extended X-ray Absorption Fine Structure (EXAFS) beamline (14 $Å^{-1}$). Then, we performed further EXAFS experiments on the classical absorption XAS13 beamline equipped with a Si 111 double monochromator. We use the fluorescence detection mode in grazing incidence, where the depth of the sample observed is limited by the escape depth of the fluorescence photons. So, the fraction of irradiated compound probed should be higher than in a classical transmission recording mode. Each EXAFS was recorded four times over a 1000 eV range, by 2 eV steps and with an integration time of 6 s per point.

The experiments were equipped with an optical fiber (light source: $h\nu$ = white light, 450 or 750 ± 50 nm; $P = 60$ mW cm^{-2}). In any case, preliminary tests were performed to determine the irradiation time after which the compound does not evolve anymore. Forty-five minutes are necessary to obtain the saturation for the soft energy experiments. For the experiments at high energy, where the signal is detected in transmission mode or in fluorescence yield, the compound has been irradiated 12 h and the saturation has not been totally reached.

XAS Data Processing. A baseline was subtracted to the $L_{2,3}$ edges below the L_3-edge region and beyond the L_2-edge region to allow comparison with the calculations.

EXAFS data analyses were performed in the frame of single scattering approximation, using the "EXAFS pour le Mac" code.[10] The EXAFS signal was extracted from the data by subtracting a linear preedge background and a combination of polynomials and cubic spline atomic absorption background and normalized by the Lengeler−Eisenberger procedure.[10] The pseudoradial distribution functions are given by the Fourier transform calculated on $w(k)k^3\chi(k)$ where $w(k)$ is a Kaiser−Bessel window with a smoothness parameter equal to 3. The k limits are equal to 2−12.5 $Å^{-1}$ ($\Delta k = 9.5$ Å) due to some Ni trace impurities in our sample. We use the FEFF7 code to calculate the amplitude and phase functions $A_j(k,\pi)$ and $\phi_{i,j}(k)$ from model compounds.[11]

Ligand Field Multiplet Calculations. To extract quantitative information from $L_{2,3}$ edges, we simulated the spectra. The calculations were performed in the so-called Ligand Field Multiplet Theory developed by Thole following Cowan and Butler.[12−14] Thole's approach takes into account all the electronic interactions and the spin−orbit coupling on any shell and treats the geometrical environment of the absorbing atom through crystal field potential.[15] In the simplest formulation, a pure $3d^n$ configuration is attributed to the ground state of the 3d transition ion. One then calculates the transitions between the $2p^63d^n$ ground state toward the $2p^53d^{n+1}$ excited states. The interelectronic repulsions are introduced through Slater integrals, F^2_{dd} and F^4_{dd} for the initial state and F^2_{pd}, G^1_{pd}, and G^3_{pd} for the final state where F and G are used to obtain the Racah parameters by linear combinations. The Slater integrals are calculated through an atomic Hartree−Fock model and they are scaled down by a reduction factor κ that depends on the electronic delocalization and on the covalence of the chemical bond. The atomic spin−orbit coupling parameters, ζ_{3d} and ζ_{2p}, are calculated through the monoelectronic potential around the ion. The octahedral surrounding of the metal ion is represented by an octahedral crystal field potential, which strength is given by the crystal field parameter 10 Dq. At this point, the covalence is only present in the calculation through the reduction parameter κ. It is not possible to take into account the charge transfer introduced by covalence. To overcome that problem one performs the same calculation by choosing a ground state that is not built from a pure configuration but is a mixture of two appropriate configurations. This is an extension of the Zaanen−Sawatzky−Allen model.[16−19] The initial ground state is taken as a linear combination of two configurations: $|\phi_i\rangle = \alpha\ |d^n\rangle + \beta|d^{n+1}\underline{L}\rangle$, where $|d^{n+1}\underline{L}\rangle$ stands for an electronic configuration with an extra d-electron (d^{n+1}) coming from the ligands L and with the corresponding hole in the ligand orbital ($\underline{L}$).[20] The charge-transfer energy is defined as $\Delta = E(d^{n+1}\underline{L}) - E(d^n)$, where $E(d^{n+1}\underline{L})$ and $E(d^n)$ are the average energies of respectively $d^{n+1}\underline{L}$ and d^n configurations. In the same way the final state is $|\phi_f\rangle = \alpha'|d^{n+1}\underline{L}\rangle + \beta'\ |d^{n+2}\underline{L}\rangle$. It follows the relation $E(2p^5d^{n+2}\underline{L}) - E(2p^5d^{n+1}) = \Delta + U_{dd} - U_{dp} = \Delta'$, where U_{dd} and U_{dp} are the average Coulomb interaction energies of the electron pairs dd and dp.[17] The strength of the covalency hybridization is represented in octahedral symmetry by V_{t2g} for the t_{2g} levels and by V_{eg} for the e_g levels where V is the ligand−metal charge-transfer integral between the $3d^n$ state and the charge-transfer $d^{n+1}\underline{L}$ state, $V = \langle 3d^n|H|3d^{n+1}\underline{L}\rangle$, H being the interaction Hamiltonian.[19] The calculation parameters are the following: Δ, Δ', V_{t2g}, and V_{eg}. Then, to take into account the resolution (intrinsic and instrumental), the calculated spectra are broadened by a Lorentzian function.

$L_{2,3}$ Edges: Results and Discussion

Model Compounds. X-ray absorption spectroscopy (XAS) of an element is sensitive to its local environment (symmetry, nature of the ligands, metal−ligand distances, and bonding), and to its oxidation and spin states. To characterize the electronic structure of the cobalt and the iron ions in the photoinduced magnetic pairs of $Rb_{0.5}CoFe$, we recorded $L_{2,3}$ edges of four relevant model compounds: $[Co^{II}(H_2O)_6](NO_3)_2$ [high spin (HS), $t_{2g}^5e_g^2$], $K_3[Co^{III}(CN)_6]$ [low spin (LS), $t_{2g}^6e_g^0$], $K_4[Fe^{II}(CN)_6]$ [LS, $t_{2g}^6e_g^0$], and $K_3[Fe^{III}(CN)_6]$ [LS, $t_{2g}^5e_g^0$], which have the electronic configurations that can be encountered in $Rb_{0.5}CoFe$. The experimental and calculated Co-$L_{2,3}$ spectra of $[Co^{II}(H_2O)_6](NO_3)_2$ and $K_3[Co^{III}(CN)_6]$ are reported in Figure 1.

The spectra of the two compounds are completely different: the spectrum of $[Co^{II}(H_2O)_6](NO_3)_2$ is characteristic of HS Co^{II} ions in octahedral symmetry.[15,20] The spectrum of $K_3[Co^{III}(CN)_6]$ is characteristic of a LS Co^{III} in octahedral symmetry.[15] All the features observed in $K_3[Co^{III}(CN)_6]$ are shifted to higher energies compared to those observed in the HS Co^{II} spectrum. This is due to the increase of the oxidation state and to the strong shortening of the Co−ligand distances in Co^{III} compared to Co^{II}.

(10) Michalowicz, A. *EXAFS pour le Mac, Logiciel pour la Chimie*; Société Française de Chimie: Paris, 1991; p 102.

(11) Zabinsky, S. I.; Rehr, J. J.; Ankudinov, A.; Albers, R. C.; Eller, M. J. *Phys. Rev. B* **1995**, *52*, 2995−3000.

(12) Cowan, R. D. *The Theory of Atomic Structure and Spectra*; University of California Press: Berkeley, 1981.

(13) Butler, P. H. *Point Group Symmetry, Applications, Methods and Tables*; Plenum: New York, 1991.

(14) Cowan, R. D. *J. Opt. Soc. Am.* **1968**, *58*, 808.

(15) (a) van der Laan, G.; Kirkman, I. W. *J. Phys: Condens. Matter* **1992**, *4*, 4189−4204. (b) van der Laan, G.; Thole, B. T. *Phys Rev. Lett.* **1988**, *60*, 1997−2000. (c) van der Laan, G. *Physica B* **1989**, *158*, 395−401.

(16) van der Laan, G.; Zaanen, J.; Sawatzky, G. A.; Karnatak, R.; Esteva, J.-M. *Phys. Rev. B* **1986**, *33*, 4253−4263.

(17) Kotani, A.; Okada, K. *Technical Report of ISSP* **1992**, Ser. A, No. 2562.

(18) Zaanen, J.; Westra, C.; Sawatzky, G. A. *Phys. Rev. B* **1986**, *33*, 8060−8073.

(19) Sawatzky, G. A. *Core-Level Spectroscopy in Condensed Systems*; Springer-Verlag: Kashikojima, 1987; 99−133.

(20) Arrio, M. A.; Sainctavit, Ph.; Cartier dit Moulin, Ch; Mallah, T.; Verdaguer, M.; Pellegrin, E.; Chen, C. T. *J. Am. Chem. Soc.* **1996**, *118* (27), 6422−6427.

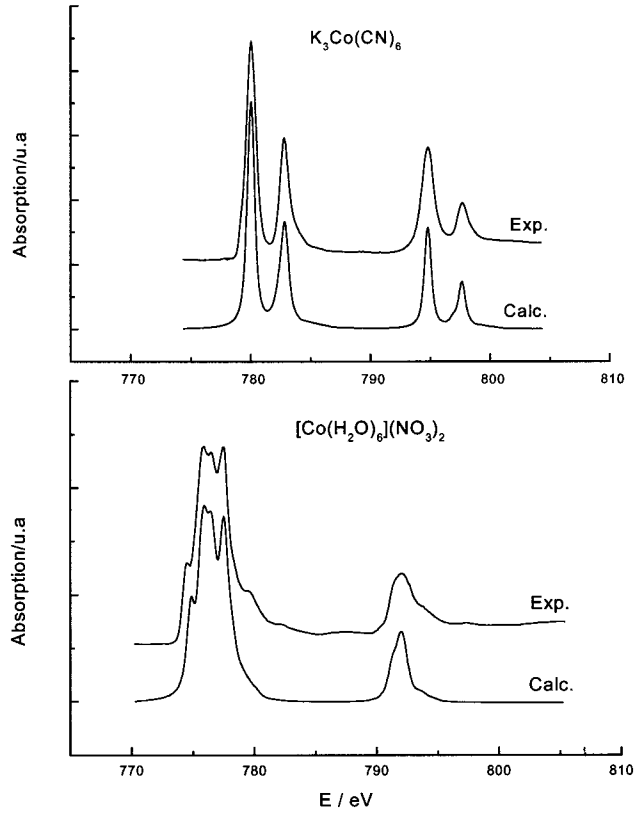

Figure 1. Experimental and calculated Co $L_{2,3}$ edges: (top) $K_3Co^{III}(CN)_6$ and (bottom) $[Co^{II}(H_2O)_6](NO_3)_2$.

The spectrum is less structured than that of HS Co^{II}, due to the lower number of multiplets expected for the $2p^5t_{2g}{}^6e_g{}^1$ configuration. The very intense band at 783 eV is the signature of the presence of the CN π^* orbitals.[21] The high intensity of the L_2 peak compared to the L_3 one is the signature of the $S = 0$ spin state.[22] The technique is therefore a priori able to distinguish clearly the two electronic structures expected in $Rb_{0.5}CoFe$. Moreover, LS Co^{II} and HS Co^{III} species would have different signatures.[15]

The Ligand Field Multiplet calculation with one configuration for the initial state and one configuration for the final state (i.e. with no interaction configuration) reproduces the most intense experimental features of the HS Co^{II} spectrum. The spin−orbit parameters used are $\zeta_{2p} = 9.75$ eV and $\zeta_{3d} = 0.022$ eV. The Slater integrals reduction factor ($\kappa = 0.8$) is close to the one used by Kotani et al. to calculate the spectra of Co^{II} dihalides.[17] This small reduction factor agrees with the weak covalent character of the $Co^{II}-O(H_2O)$ bond. The κ factor is comparable to the $\beta = B/B_o$ parameter used in optical spectroscopy for ordering the nephelauxetic series, where B and B_o are the Racah parameters for the complex and the free ion, respectively.[23] For the $[Co^{II}(H_2O)_6](NO_3)_2$ complex, $B = 780$ cm^{-1} and $B_o = 971$ cm^{-1},[23] the $\beta = 0.8$ value found is equal to the κ for our calculation. The crystal field parameter is found as 10Dq = 1.0 eV in fair agreement with optical spectroscopy (10Dq = 0.9 eV).[23] A similar calculation based on one configuration is unable to reproduce the experimental spectrum of $K_3[Co^{III}(CN)_6]$. κ has to be decreased compared to the previous calculation to take into account the strong covalence of the Co−CN bond, as can be expected from the nephelauxetic series.[23]

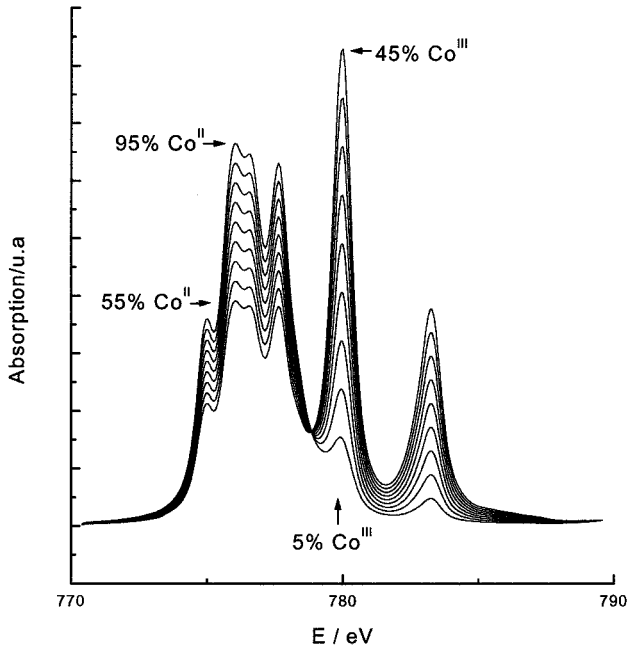

Figure 2. Linear combinations of the calculated Co L_3 edges for $K_3[Co^{III}(CN)_6]$ and $[Co^{II}(H_2O)_6](NO_3)_2$ varying the percentage of LS Co^{III} from 5 to 45% (step 5%).

10Dq has to be increased. Configuration interaction is needed to take into account the metal−ligand charge transfer, due to the existence of a large π back-bonding with C-bonded CN ligands. The expression of the initial state is then written $|\phi_i\rangle = \alpha|d^n\rangle + \beta|d^{n-1}L^1\rangle$ to model the Co−CN bond by mixing $|3d^6\rangle$ and $|3d^5L^1\rangle$.

The parameters of the calculations are the following: $\kappa = 0.50$, 10Dq = 3.0 eV, $\Delta = 3.0$ eV, $\Delta' = 2.0$ eV, $V_{t2g}/V_{eg} = -1.5$, $n_{eff} = 5.87$ (n_{eff} is the effective number of 3d electrons). We used previously the same approach to calculate the Cr-$L_{2,3}$ edges in $K_3Cr^{III}(CN)_6$ detailed elsewhere.[20] The parameters κ and 10Dq of the Cr and Co $L_{2,3}$ edge calculations are close, which reflects the similarity of the M−CN bonds and confirms the validity of the parameters used. The effective number of d electrons n_{eff} found to be 5.87 reflects a 0.13 electron transfer to the cyanide orbitals through π back-bonding.

The calculations give the absolute intensity of the absorption signal for the two cobalt configurations which can be present in our samples. They can be used to extract from the experimental spectra the fractions of HS Co^{II} and LS Co^{III} in the material, by computing linear combinations of the calculated spectra in which the percentage of the two configurations is varied (Figure 2).

The intensity ratio of the well-resolved experimental peaks at 777.6 (HS Co^{II}) and 780 eV (LS Co^{III}) gives the percentage of the two species present in the material, by comparison with the calculated linear combinations.

The experimental Fe-$L_{2,3}$ spectra for $K_4[Fe^{II}(CN)_6]$ [LS, $t_{2g}{}^6e_g{}^0$] and $K_3[Fe^{III}(CN)_6]$ [LS, $t_{2g}{}^5e_g{}^0$] are reported in Figure 3.

The first peak at 704.5 eV is observed in the Fe^{III} derivative but not in the Fe^{II} one. It corresponds to the excitation $2p^6t_{2g}{}^5 \rightarrow 2p^5t_{2g}{}^6$ absent in the LS Fe^{II} configuration ($t_{2g}{}^6$ ground state). This peak is the signature of the LS Fe^{III} configuration.[24] The other peaks between 707 and 715 eV correspond to multiplet

(21) Arrio, M. A.; Sainctavit, Ph.; Cartier dit Moulin, Ch.; Brouder, Ch.; de Groot, F. M. F.; Mallah, T.; Verdaguer, M. *J. Phys. Chem.* **1996**, *100*, 4679−4684.

(22) Thole, B. T.; Van der Laan, G. *Phys. Rev. B* **1988**, *38*, 3158.

(23) Lever, A. B. P. *Inorganic electronic spectroscopy*, 2nd ed.; Amsterdam: Elsevier: 1984; pp 115 and 483.

(24) Cartier dit Moulin, C.; Rudolf, P.; Flank, A.-M.; Chen, C. T. *J. Phys. Chem.* **1992**, *96*, 6196−6198.

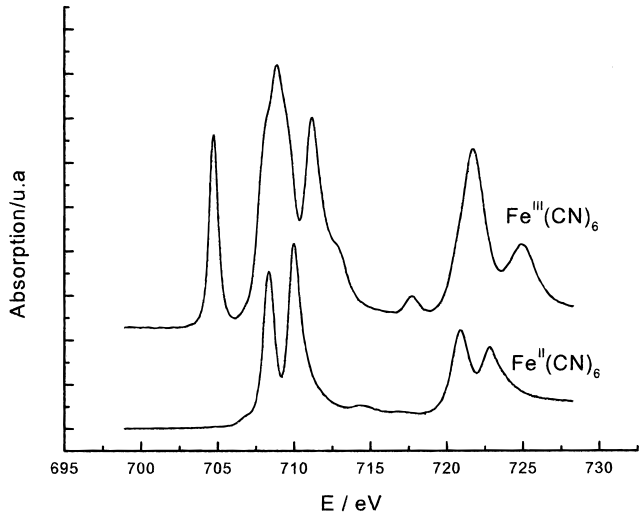

Figure 3. Experimental $L_{2,3}$-Fe edges for $K_4[Fe^{II}(CN)_6]$ and $K_3[Fe^{III}(CN)_6]$.

structures arising from transitions from 2p to e_g orbitals. Except for the peak at 704.5 eV, the transitions of Fe^{II} and Fe^{III} are located in overlapping energy ranges and the electronic transfer to evidence will appear less clearly than at the Co L edges. As for the cobalt model compounds, we performed the calculation of the iron $L_{2,3}$ edges. To date, we have not obtained a good agreement between experimental and calculated spectra for both $K_4[Fe^{II}(CN)_6]$ and $K_3[Fe^{III}(CN)_6]$ model compounds. This work is still underway. Nevertheless, given the overlap of the transitions, the extraction of quantitative information will be difficult at the iron edge. We qualitatively follow instead the $Fe^{II} \rightarrow Fe^{III}$ transformation looking at the intensity of the 704.5 eV peak.

$Rb_{0.5}$CoFe Metastable State. The Co and Fe $L_{2,3}$ edges for $Rb_{0.5}$CoFe recorded at room temperature and at 20 K after 45 min of irradiation are reported in Figure 4. Figure 4a shows the Co edges. The ground state of the compound, at room temperature is a mixture of Co^{II} [HS, $t_{2g}^5e_g^2$] and Co^{III} [LS, $t_{2g}^6e_g^0$] species. Measuring the relative intensities of the peaks at 777.6 (HS Co^{II}) and 780 eV (LS Co^{III}), the percentage of the LS Co^{III} species, expected to give rise to the photomagnetic effect, can be estimated as 28%. This value is weak, compared to that given by the chemical formula (82.5%). The difference is not unexpected since the detection mode probes the surface of the particles, different from the bulk and richer in HS Co^{II} sites (maybe adsorbed unreacted Co^{II} ions).

The spectrum obtained after irradiation displays a decrease of the signal of the LS Co^{III} species and a simultaneous increase of the signal of the HS Co^{II} species. The light induces the transformation of Co^{III} in Co^{II} ions accompanied by a spin change of the Co ions. Indeed, a LS Co^{II} species would have a completely different signature not observed here.[15a] More precisely, the branching ratio B, defined as $B = I_{L3}/(I_{L2} + I_{L3})$ (I_{L3} and I_{L2} are the integrated intensities of the L_3 and L_2 edges), depends on the spin state of the metallic ion.[15b,c,25] The calculated values of B are 0.78 for the HS Co^{II} ion ($S = 3/2$) and 0.66 for the LS Co^{II} ion ($S = {}^1/_2$).[15b,c] In $Rb_{0.5}$CoFe, it is not possible to extract the branching ratio of Co^{II}, because of the presence of Co^{III}. Nevertheless, an estimation of B can be provided by $B(Co^{II}) \approx I_{max}(Co^{II})_{L3}/(I_{max}(Co^{II})_{L2} + I_{max}(Co^{II})_{L3})$. In $[Co^{II}(H_2O)_6](NO_3)_2$, the approximate value is $B(Co^{II}) = 0.76$, close to the expected 0.78. For $Rb_{0.5}$CoFe before irradiation,

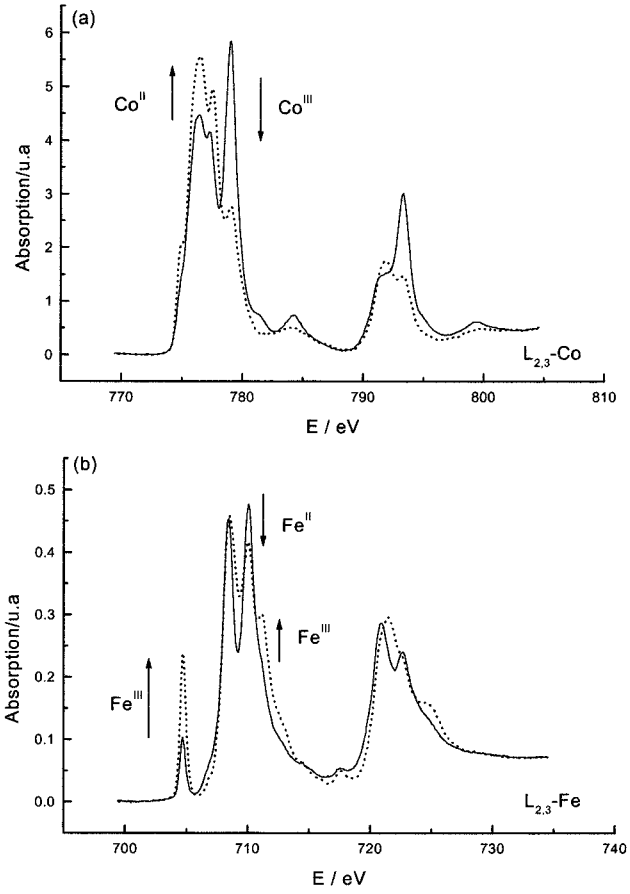

Figure 4. (a) Co-$L_{2,3}$ edges and (b) Fe-$L_{2,3}$ edges for $Rb_{0.5}$CoFe: (—) at 300 K before irradiation and (- - -) at 20K after 15 min of irradiation time ($h\nu = 750 \pm 50$ nm).

we obtained $B(Co^{II}) = 0.74$, which indicates a high spin configuration. After irradiation, we found $B(Co^{II}) = 0.76$, which confirms that the photocreated Co^{II} ions are also high spin.

The Fe $L_{2,3}$ edges spectra are reported in Figure 4b. Before irradiation, the presence of the 704.5 eV feature shows the presence of LS Fe^{III} entities at the surface of the particles, in line with the presence of Co^{II} and Co^{III} entities found at the Co $L_{2,3}$ edges. After irradiation, the intensity of the 704.5 eV peak increases as the LS Fe^{II} proceeds to LS Fe^{III} transformation, in agreement with the Co $L_{2,3}$ edges changes.

The above data obtained by a local probe of the metallic d orbitals are the first direct evidence of the light induced electronic transfer $Fe^{II}Co^{III} \rightarrow Fe^{III}Co^{II}$ with a LS $\rightarrow$ HS spin change of the Co ions, initially postulated to explain the changes in the macroscopic magnetic properties of the material.

To go further and to quantify the changes observed at the Co-$L_{2,3}$ edges, Figure 5 shows the decrease of the Co^{III} fraction computed from the Co-L_3 edges during the irradiation.

Very rapidly (in 10 min), an important portion of the LS Co^{III} ions is transformed into HS Co^{II}. After 45 min of irradiation, 13% of the Co atoms are still LS Co^{III} and remain unchanged for longer irradiation time. The light induces the transformation of 54% of Co^{III} to Co^{II} ions (from 28 to 13%). The penetration depth of the visible light, larger than the escape depth of the electrons, ensures that the atoms we look at all have been irradiated. The conclusion is that 46% of the diamagnetic pairs, at the surface of the grains, remains unchanged. We can then distinguish between two types of diamagnetic pairs: light induced transformable pairs (54%) and inactive pairs (46%). Our hypothesis is that the inactive pairs are in an environment

(25) Yokoyama, T.; Ohta, T.; Sato, O.; Hashimoto, K. *Phys. Rev. B* **1998**, *58*, 8257−8266.

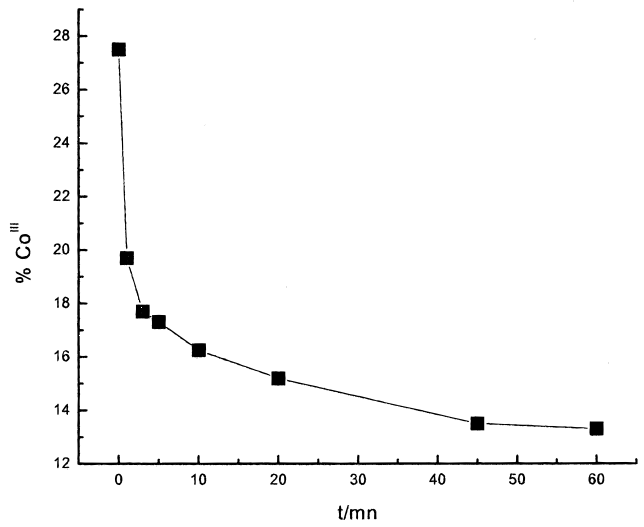

Figure 5. Evolution of the Co^{III} percentage with the irradiation duration ($h\nu = 750 \pm 50$ nm).

comparable to those of $CsCoFe(CN)_6$, i.e., an environment with no or few $Fe(CN)_6$ vacancies, for which no light-induced electron transfer was observed.[7] Another important observation is that no change in the spectra occurs several hours after the end of the irradiation. That means that the magnetic pairs formed are stable at $T = 20$ K, even at the surface of the grains.

In another material of the same family, Sato et al. observed that irradiation with blue light decreases the magnetization first created by red light.[1] We did the same experiment on $Rb_{0.5}CoFe$. First, we irradiated for 10 min with red light ($h\nu = 750 \pm 50$ nm) to transform an important portion of diamagnetic pairs but not all of them. Then, we irradiated the sample 10 min with blue light ($h\nu = 450 \pm 50$ nm) and we observe, contrary to the precedent observation, a further transformation of the diamagnetic pairs. So, we exposed our compound to blue radiation with no previous red irradiation. After 15 min of illumination, we also observed the transformation of 38% of diamagnetic pairs into magnetic ones as with red light. The transformation fraction is less important than the one obtained with red light (44%) but remains high. We verify also that irradiation with white light induces also the electron transfer. It results that there is not only one excited state with a well-defined energy: (i) the material contains different diamagnetic pairs with various environments for the Co^{III} ions, giving excited states with different energies, and (ii) for each kind of pairs, several excited Franck−Condon states are present. The result shows the complexity of the atomic local arrangement in the material.

Cobalt K-Edge: Results and Discussion

The electronic transfer has also been followed using the XANES part of the Co K-edge spectrum. The Co K-edge XANES spectra recorded at room temperature and after irradiation ($h\nu = 750 \pm 50$ nm during 12 h, $T = 30$ K) are reported in Figure 6. The experimental geometry of the energy dispersive beamline where the spectra have been recorded increases the percentage of irradiated compound, because of the small quantity of product needed (≈2 mg) compared to a classical X-ray absorption setup (≈20 mg). The irradiation induces a 1.5 eV low-energy shift of the absorption maximum and a 1 eV shift for the preedge from 7711 to 7710 eV. These shifts evidence the decrease of the cobalt oxidation state from III to II, induced by irradiation.[7] The low-energy shift of the first EXAFS

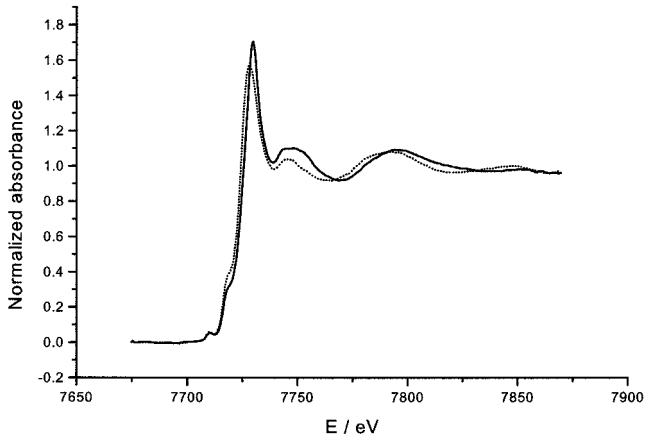

Figure 6. Co K-edge XANES spectra for $Rb_{0.5}CoFe$: (—) at 300 K before irradiation and (- - -) at 30 K after 12 h of irradiation time ($h\nu = 750 \pm 50$ nm).

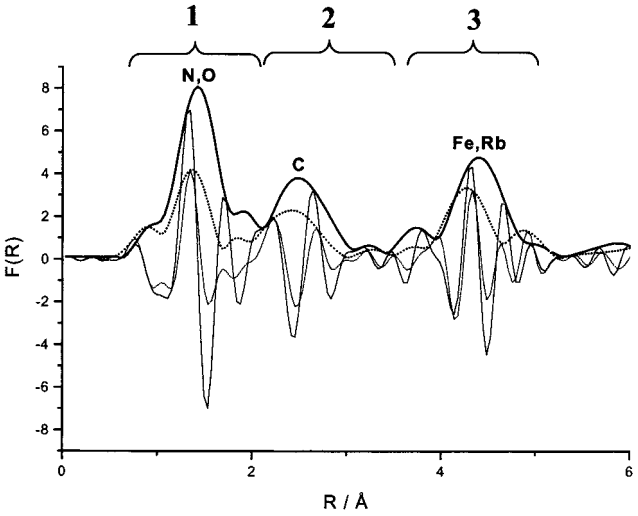

Figure 7. Fourier transform moduli and imaginary parts of EXAFS signals measured at the Co K edge for $Rb_{0.5}CoFe$: (—) at 300 K before irradiation and (- - -) at 30 K after 12 h of irradiation time ($h\nu = 750 \pm 50$ nm) (bold for moduli).

oscillation at 7790 eV is due to the increase of the Co−ligand distances, associated with the $Co^{III} \rightarrow Co^{II}$ transformation. The result confirms qualitatively those obtained at the Co $L_{2,3}$ edges. The disadvantage of the dispersive recording mode is the reduced energy range scanned, which makes impossible the quantitative analysis of the EXAFS part of the spectra. So, we performed the same experiment on a beamline equipped with a classical step-by-step mode and a fluorescence detector to obtain the EXAFS spectra on a larger energy range.

In Figure 7 are reported the Fourier transform moduli and imaginary parts of the EXAFS signals recorded at the Co K-edge before and after irradiation ($h\nu = 750$ nm during 12 h, $T = 30$ K). In the ground state, the Fourier transform modulus presents three peaks attributed to the three first shells around the cobalt, O and N, C from the NC ligands, and Fe and Rb atoms. After irradiation, we observe important changes, which are difficult to analyze. Even if the linear geometry of the Fe−CN−Co entities introduces strong multiple scattering phenomena in the EXAFS signal[25,26] and impedes a straightforward immediate analysis, the first peak and its changes (intensity and shift) can be analyzed in terms of single scattering. Nevertheless, the first

(26) Giorgietti, M.; Berrettoni, M.; Filipponi, A.; Kulesza, P. J.; Marassi, R. *Chem. Phys. Lett.* **1997**, *275*, 108−112.

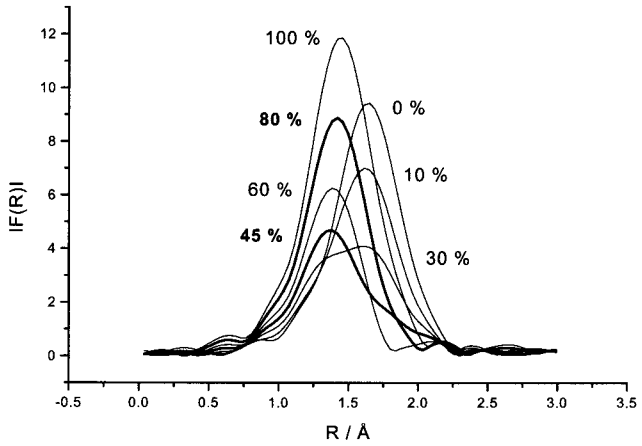

Figure 8. Fourier transform moduli of the linear combinations of EXAFS signals calculated for the two reference cobalt sites Co-L_6 at 2.08 and 1.91 Å and various percentages of each contribution. The numbers refer to the short distance contribution percentage.

and second peaks are not resolved enough to be separately analyzed and it was not possible to fit the first shell with classical procedures. Peak 1 (Figure 7) corresponds to the sum of the mean cobalt atoms Co-L_6 (L = N, O). This peak is not well separated from the second one, which corresponds to the contributions of the carbon atoms second neighbors. Nevertheless, quantitative information on the coordination sphere of the cobalt atom can be extracted from peak 1. To do that, we calculate the EXAFS signals for cobalt octahedral environments: 6 O/N neighbors at 2.08 Å, typical distance for HS Co^{II} ions,[26] and 6 O/N neighbors at 1.91 Å, typical distance for LS Co^{III} ions.[27,28] These distances were also obtained by Hashimoto et al. for analogues compounds.[25] EXAFS signals have been calculated in the single scattering approximation with amplitude and phase shift functions calculated by the FEFF7 code for an octahedral CoN_6 cluster (Co−N = 1.91 Å).[11] Linear combinations of those signals have been performed varying the percentages of the two contributions. The Fourier transform moduli of the linear combinations are reported in Figure 8, from 100% of the short distance contribution (when all the Co ions are LS Co^{III}) to 0% (when all the Co ions are HS Co^{II} ions).

First, from 100 to 45%, we observe a decrease of the intensity accompanied by a shift to lower distance whereas the fraction of long distances increases. The same shift is also observed on the experimental Fourier transform modulus of the compound after irradiation (Figure 7), which indicates an increase of the Co-L_6 long distance fraction. We can note that the imaginary part (Figure 7) is shifted to higher distances, which directly reflects the long distance fraction increase. Second, from 45 to 0%, an increase of the intensity and a shift to higher distance is observed. Given the important difference between the two distances, the change is clearly observed. Comparison between the calculated linear combinations and the experimental Fourier transform moduli allows an accurate determination of the fraction of each species present in the compound. In the ground state, the best agreement (position and intensity of the peak) is obtained for 80% of d_{Co-L} = 1.91 Å distances and 20% of d_{Co-L} = 2.08 Å. These values are in agreement with the chemical formula ($Rb_{0.5}CoFe$) corresponding to 82.5% of Fe^{II}−CN−Co^{III} diamagnetic pairs (with short Co−N bonds) and 17.5% of Co^{II}−iron vacancy (with long Co−N/O bonds). After irradiation, we found only 45% of Co atoms with short Co−L_6 distances, i.e., 55% (45/80 × 100) of the Co^{III} ions have been transformed into Co^{II}. The result shows that the photoinduced electron transfer is associated with a local structural rearrangement of the coordination sphere of the concerned cobalt ions. The 0.17 Å bond lengthening, which is quite large, has to be absorbed by the inorganic three-dimensional network, which should induce strong network strains.

The electronic and the local structure of the Fe^{III}−CN−Co^{II} magnetic pairs, either photoinduced or present in the ground state of compounds such as $K_{0.1}Co_4[Fe(CN)_6]_{2.7}\cdot 18.4H_2O$, are identical below the thermal relaxation temperature. Then, the magnetic coupling constant J values are the same, which confirms that the increase of the Curie temperature expected in the photoinduced state is effectively due to the increase of the number of magnetic neighbors.[7] Furthermore, as the compound $K_{0.1}Co_4[Fe(CN)_6]_{2.7}\cdot 18.4H_2O$ is ferrimagnetic below the Curie temperature, the irradiated compound $Rb_{1.8}Co_4[Fe(CN)_6]_{3.3}\cdot 13H_2O$ should be ferrimagnetic as well. This is not surprising with two ferromagnetic (t_{2g}−e_g) and one antiferromagnetic (t_{2g}−t_{2g}) exchange paths.[29] But this would not have been the case if the photoinduced Co^{II} ions were low spin. The low-spin Co^{II} ions have not been evidenced by the XAS measurements.

Conclusions

Our study confirms experimentally the explanation of the photoinduced magnetization previously proposed.[1,5,6] To the best of our knowledge this is the first experimental local and direct evidence on the two metallic sites of a photoinduced metal-to-metal electron transfer in a three-dimensional compound:

$$Fe^{II}(LS)-CN-Co^{III}(LS) \rightarrow Fe^{III}(LS)-CN-Co^{II}(HS)$$

The photoinduced magnetic domains are generated through the molecular excitation of diamagnetic pairs Fe^{II}−CN−Co^{III}.

Three-dimensional ferrimagnetic domains are created under light but all the initial diamagnetic pairs are not transformed into ferrimagnetic ones. At the surface, as well as in the bulk of the material, about 50% of the diamagnetic pairs remain diamagnetic. We propose that their nature is the same as the nonexcitable diamagnetic pairs in $Cs_{3.9}Co_4[Fe(CN)_6]_{3.9}\cdot 12.9H_2O$. The electron transfer is accompanied by a bond lengthening that has to be taken up by the inorganic network. In a perfect structure without vacancies, strains in the bulk are strong so that only diamagnetic pairs at the surface of the compound can be transformed. The forces generated in the bulk by the bond lengthening tend to cancel each other since all cobalt atoms are surrounded by iron−cobalt pairs. On the opposite side, in a structure with vacancies, the steric strains are weaker, the network is more flexible, and the photoinduced metastable state is able to propagate in the bulk. In our interpretation, the diamagnetic pairs close to iron vacancies would be photosensitive. The other pairs trapped in a more compact local structure would be inert to photons. The efficiency of the photoinduced magnetization should then depend on a compromise between the number of diamagnetic pairs and vacancies in the structure. This point will be discussed in a following paper.

Acknowledgment. We thank A. Goujon and F. Varret for valuable discussions and help in the irradiation of the sample and the European Community (Grant ERBFMRXCT980181) and the CNRS (Program Matériaux) for financial support.

JA000349M

(27) Morales, A. D.; Romero, R. G.; Rodriguez, J. D.; Hernandez, R. P.; Bertran, J. F. *Transition Met. Chem.* **1990**, *15*, 106−108.

(28) Roux, C.; Adams, D. M.; Itié, J. P.; Polian, A.; Hendrickson, D.; Verdaguer, M. *Inorg. Chem.* **1996**, *35*, 2846−2852.

(29) Mallah, T.; Thiébaut, S.; Verdaguer, M.; Veillet, P. *Science* **1993**, *262*, 1554−1557.